energies

MDPI

Article

Expansion of High Efficiency Region of Wind Energy Centrifugal Pump Based on Factorial Experiment Design and Computational Fluid Dynamics

Wei Li [1,*], Leilei Ji [1], Weidong Shi [2,*], Ling Zhou [1], Hao Chang [1] and Ramesh K. Agarwal [3]

1 Research Center of Fluid Machinery Engineering and Technology, Jiangsu University, No.301, Xuefu Road, Jingkou District, Zhenjiang 212013, China; jileileidemail@163.com (L.J.); lingzhoo@hotmail.com (L.Z.); changhao1514@163.com (H.C.)

2 College of Mechanical Engineering, Nantong University, No.9 Se Yuan Road, Chongchuan District, Nantong 226019, China

3 Department of Mechanical Engineering & Materials Science, Washington University in St. Louis, St. Louis, MO 63130, USA; rka@wustl.edu

* Correspondence: lwjiangda@ujs.edu.cn (W.L.); wdshi@ujs.edu.cn (W.S.); Tel.: +86-137-7555-4729 (W.L.); +86-135-0528-8312 (W.S.)

Received: 24 December 2019; Accepted: 12 January 2020; Published: 19 January 2020

Abstract: The wind energy pump system is a new green energy technology. The wide high efficiency region of pump is of great significance for energy conservation of wind power pumping system. In this study, factorial experiment design (FED) and computational fluid dynamics (CFD) are employed to optimize the hydraulic design of wind energy centrifugal pump (WECP). The blade outlet width b_2, blade outlet angle β_2, and blade wrap angle ψ are chosen as factors of FED. The effect of the factors on the efficiency under the conditions of $0.6Q_{des}$, $0.8Q_{des}$, $1.0Q_{des}$, and $1.4Q_{des}$ is systematically analyzed. The matching feature of various volute tongue angle with the optimized impeller is also investigated numerically and experimentally. After the optimization, the pump head changes smoothly during full range of flow condition and the high efficiency region is effectively improved. The weighted average efficiency of four conditions increases by 2.55%, which broadens the high efficiency region of WECP globally. Besides, the highest efficiency point moves towards the large flow conditions. The research results provide references for expanding the efficient operation region of WECP.

Keywords: wind energy centrifugal pump (WECP); factorial experiment design (FED); optimization; high efficiency area; computational fluid dynamics (CFD)

1. Introduction

The WECP system is a new green energy technology that converts wind energy into electric energy firstly and then uses the battery to drive the pump. At present, the focus of wind power extraction system research is mainly on the performance improvement of wind turbine and the technology of frequency conversion control, whereas the match between pump and system is not well investigated. As wind energy is the variation of solar energy, the wind speed, wind direction, and energy vary with season, altitude, region, and surface coarseness, representing the great change of power generated by wind turbines (the input power of motor). Therefore, the operating condition of wind pump is in variation. The traditional design method of vaned pump will not satisfy the requirements of ultra-wide operating condition of WECP [1–3]. Therefore, it is urgent to expand the high efficiency region of WECPs, improve the efficiency of pump system, and optimize the matching characteristics of volute and impeller, which is of great significance for energy conservation and consumption reduction of wind power pumping system.

Clark R N et al. [4–6] carried out a detailed study on the performance of the small wind power pump and the electric design method of the wind energy pump system. Based on the main composition and principle of the research system, Zhu et al. [7] analyzed the matching optimization of the generator and pump and carried out a test on a wind power pumping system. Lin et al. [8] experimentally simulated the wind power water pumping system and revealed the relationship between flow rate and head power under different wind speeds. However, the focus of above researches is on the performance of wind power pump water system and the matching between generator and pump. It is not specifically designed to improve the performance of pump devices, which could be matched with the wind machinery, especially the performance of the wind power centrifugal pump under the non-design condition. Following are the methods for the performance optimization of centrifugal pumps, namely, loss extreme method, criterion screening method, CFD optimization design method, and experimental design method. The loss extreme method is used to solve the combination of pump geometry parameters that meet the performance to minimize pump losses for optimum performance indicators under the condition of ensuring the flow rate and head of the design working point. Li et al. [9] extended the method of Neumann [10] to the design of all vane pumps. He combined various losses as the minimum principle in the design to ensure the dimensions of components match with each other, analyzed the flow of vane pump under non-design conditions, and proposed the corrective action. Gao and Guo et al. [11] analyzed the influence of impeller and volute design parameters on pump performance, constructed a multi-objective calculation model to solve a set of design parameters by using the highest efficiency and optimal cavitation performance of centrifugal pumps as the objective function, and verified its correctness through instances. Tan et al. [12] analyzed the problems existing in the centrifugal pump hydraulic loss analysis method and gave an expression for the loss coefficient of each component in the form of using specific speed as an independent variable through theoretical analysis. The criterion screening method is proposed for the shortcomings of loss extreme method; the level of optimization depends on whether the criteria are reasonable. Based on the analysis of internal flow mechanism of centrifugal impeller, the criterion screening method established an objective function that reduces losses and achieves performance metrics, sought a combination of geometric parameters of overcurrent components, and screened out the best solution. However, these traditional vane pump optimal operating point design methods cannot meet the requirements of ultrawide operating conditions of WECPs.

CFD optimization is to guide the pump optimization through the simulation of three-dimensional incompressible flow field of pumps by means of high-performance computer [13–16]. In recent years, researchers have developed this method firstly on the preliminary design with one-dimensional theory and then CFD optimization. Goto et al. [17] presented the hydraulic design method of centrifugal impeller based on the whole three-dimensional inverse problem design. Passrucker et al. [18] designed inversely the axial plane projection and blade molded line of impeller by using CFD. Zhou et al. [19] simulated the internal flow of a new type of three-dimensional surface return diffuser to improve the hydrodynamic performance of the deep-well centrifugal pump. Although this method is very convenient to optimize the pump efficiency, it entirely relies on the high-performance computer and experienced technicians using CFD.

Experimental design is a mathematical statistical method for arranging test and analyzing test data. The commonly used experimental design methods are orthogonal test design, FED, response surface design, etc. [20]. The design theory of pump greatly dependent on experience is still not perfect yet. In the optimal design of pumps, the orthogonal test design method is widely adopted. According to the design requirements of non-overload centrifugal pump, Yuan et al. [21] analyzed the effect of geometric parameters on pump efficiency as well as head and shaft power, and they have figured out the main factors based on the orthogonal test. The orthogonal test design of a deep well pump was carried out by Shi et al. [22]. As a result, the influence of design parameters on pump performance was analyzed to find out the significant and nonsignificant factors affecting the pump performance and obtain a better design scheme. Wang et al. [23] carried out a test optimization design for a vortex

pump, and the results have been improved greatly. It is proved that the test design is of reference value for the optimization design of pump. The orthogonal test design is easy to obtain the main effect of all factors, but the optimal scheme can only be a combination of the level used in the experiment, and the optimization results will not exceed the range of the taken level. The FED, also known as the full FED, has the advantages of finding main effects from various factors and analyzing the interaction effects between various factors. In medical research, FED is used to select the best treatment scheme and adjust the drug formula, but the optimization design of FED used in the pump is rarely reported [24].

These related studies reveal that these four optimization methods have their own pros and cons. Loss extreme method and criterion screening method are the design methods for the majorization of operating point, which is not applicable for the design of WECPs with wide high efficiency region. Test optimization is accurate and reliable, but it is time-consuming and resource-consuming. CFD optimization is not restricted by physical model and test apparatus, which saves time and money substantially [25–27]. However, due to the lack of standards for judging whether CFD results are accurate or not, it needs to be validated against experimental results. Therefore, in this paper, we propose to combine the FED optimization and CFD optimization together, namely, FED-CFD. By employing numerical simulations and taking the efficiency and head of centrifugal pump under different operating points as the design indexes, the optimal parameter combination is obtained to efficiently match the volute. The optimal design was obtained by FED-CFD method (combination of FED and CFD method) and verified by prototype test. This paper could provide guidance for the optimization of multi condition centrifugal pumps.

2. Hydraulic Design of WECP

2.1. Model Design Requirements

Because of abrupt change of operating conditions of WECP, the primary goal of WECP is to maximize the average efficiency of pump within full range of flow rate conditions; that is, the WECP should have a wider high efficiency region. The traditional design method of pump will not satisfy the requirements of ultrawide operating condition of WECP. When the pump operates under nonoptimized condition, the performance decreases sharply and the constant operation will cause the pump unit instability. Therefore, to improve the overall efficiency of WECP and expand the high efficiency region of WECP, the impeller structure should be optimized based on FED-CFD method. In this paper, the parameters of WECP model are as follows: specific speed n_s = 68, designed flow rate Q = 22 m^3/h, designed head H = 11 m and rotational speed n = 1450 r/min.

2.2. Original Parameter Selection

According to the basic pump equation and the infinite blade number hypothesis, the theory head of impeller and the circumferential velocity component of impeller outlet could be expressed as follows,

$$H_{T_\infty} = \frac{u_2^2}{g}\left(1 - \frac{Q}{\pi u_2 D_2 b_2 \psi_2 \eta_V}\right) \tag{1}$$

$$u_2 = \frac{\pi D_2 n}{60} \tag{2}$$

To keep the original model pump unchanged, the inlet and outlet diameters of impeller are not changed. After transformation, the calculation formula of head is as follows,

$$H_{T_\infty} = \frac{1}{g}\left(\frac{\pi^2 D_2^2}{60^2}\right)n^2 - \left(\frac{n}{60 g b_2 \psi_2 \eta_V}\right)\cot\beta_2 nQ \tag{3}$$

The slope of head curve is obtained by Equation (4),

$$\varphi = \frac{n}{60gb_2\psi_2}\cot\beta_2 \tag{4}$$

Thus, the pump efficiency could be derived by the above equations as follows,

$$\eta = \frac{\rho gQH}{P} \tag{5}$$

where φ is the slope of head curve, dimensionless; b_2 is the blade outlet width (mm); β_2 is the blade outlet angle (°); ψ is the blade wrap angle (°); n is the impeller speed (r/min); g is the gravitational acceleration (m/s^2); $H_{T\infty}$ is the theoretical head (m); Q is the flow rate (m^3/s); D_2 is the outer diameter of the impeller (m); η_v is hydraulic efficiency, dimensionless; and η is pump efficiency, dimensionless. Formula (4) shows that, without changing the inlet and outlet diameter of impeller, the width of blade outlet width b_2, the blade outlet angle β_2, and the blade wrap angle ψ can be used as the adjusting factors to optimize the energy performance of multi-condition of WECP. The definition of impeller key parameters is shown in Figure 1. The axial projection is shown in the left figure and the plane projection is shown in the right figure. The middle streamline *a*-*b*-*c* in the axial projection corresponds to the middle line *a*′-*b*′-*c*′ on the blade surface. According to the relevant empirical parameters and combined with the original model hydraulic size, the range of values of these three variables is specified, and the combination of impeller parameters under three different variables is set as the initial factor of FED, as shown in Table 1. Among them, each factor is given two levels, and the code is set according to the level, the low level is set to −1, the high level is set to +1, and the center point is set to 0.

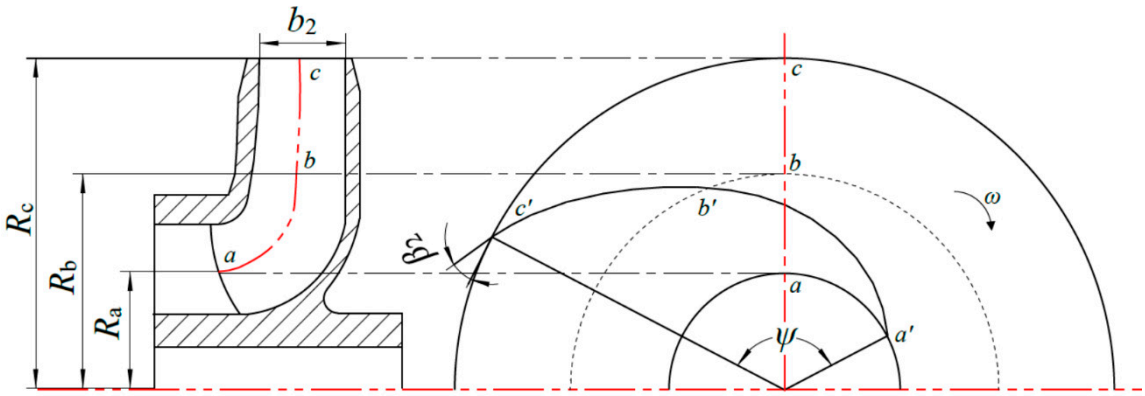

Figure 1. Definition of key parameters.

Table 1. Factor settings.

Independent Variable Factor	−1	0	1
Outlet width of the impeller blade b_2/mm	19	21	23
Outlet angle of the impeller blade β_2/°	16	19	22
Wrap angle of the impeller blade ψ/°	150	160	170

Considering that several factors are implemented simultaneously in the experiment, there may be interactions between factors, so the full FED is selected for analysis [28]. To achieve the principle of "trial repetition", we should arrange repeat tests at the "central point". To ensure repeatability with as few test times as possible, three trials were performed at the center point. A total of 26 (= 23 + 3) trials are conducted. The "center point" of this paper is Impeller 1, Impeller 7, and Impeller 8, respectively. The experiment strategy is shown in Table 2. In the table, A is the blade outlet width b_2, B is the blade outlet angle β_2, and C is the blade wrap angle ψ.

Table 2. Scheduling.

Order of Impeller	Center Point	A	B	C
1	0	0	0	0
2	1	−1	−1	1
3	1	−1	1	−1
4	1	1	−1	−1
5	1	1	−1	1
6	1	−1	1	1
7	0	0	0	0
8	0	0	0	0
9	1	1	1	−1
10	1	1	1	1
11	1	−1	−1	−1

2.3. Hydraulic Design and Establishment of Original Model

The hydraulic design of impeller is carried out by means of PCAD software, and other geometric parameters are kept unchanged during parameter setting. According to the combination of Table 3, the blade outlet width b_2, the blade outlet angle β_2, and the blade wrap angle ψ are designed. The hydraulic model diagram of 11 sets of schemes is designed. Then the 3D geometric model is constructed by using Pro/E. The central point is the hydraulic model of Impeller 1, as shown in Figure 2.

Table 3. Basic geometric parameters of the pump.

Geometric Parameter	Value
Inlet diameter of the impeller D_1 (mm)	62.5
Hub diameter of the impeller D_{hb} (mm)	20
Outlet diameter of the impeller D_2 (mm)	185
Inlet angle of the impeller blade β_1 (°)	14
Outlet angle of the impeller blade β_2 (°)	19
Wrap angle of the impeller blade ψ (°)	160
Number of the impeller blades Z	6
Outlet width of the impeller blade b_2 (mm)	21
Rotate speed n (r/min)	1450
Designed flow Q_{des} (m^3/h)	22
Specific speed n_s	68
Designed Head of delivery H (m)	11

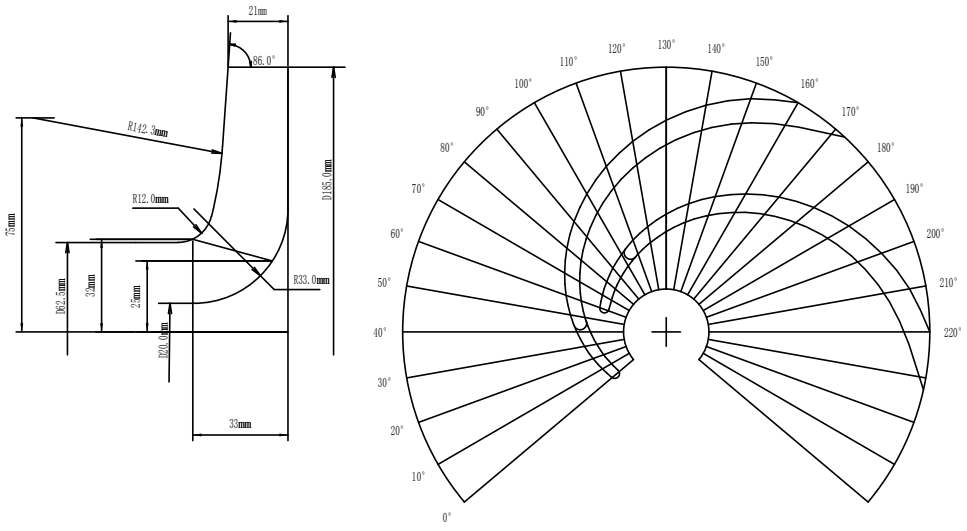

Figure 2. Hydraulic model of Impeller 1.

3. Prediction of Energy Performance and High Efficiency Region

CFD numerical simulation is used to predict the energy performance and high efficiency region of WECP, to select the most optimal scheme. First, the 3D geometric calculation model is constructed, and then the appropriate mesh is generated and imported into ANSYS CFX for the numerical calculation. Although CFD is suitable for simulating the internal flow field of rotating machinery, the numerical settings of CFD should be selected appropriately to ensure the reliability of results. Therefore, a series of numerical calculations for WECP are performed using different grid numbers, turbulence models, and convergence precisions.

3.1. Establishment of the Calculation Domain

Pro/E software has been used to conduct 3D simulation domain of the inlet (semi-spiral suction chamber), impeller, volute, and the front and rear chamber of the model pump, to obtain the 3D mode of whole calculation area of WECP, see Figure 3.

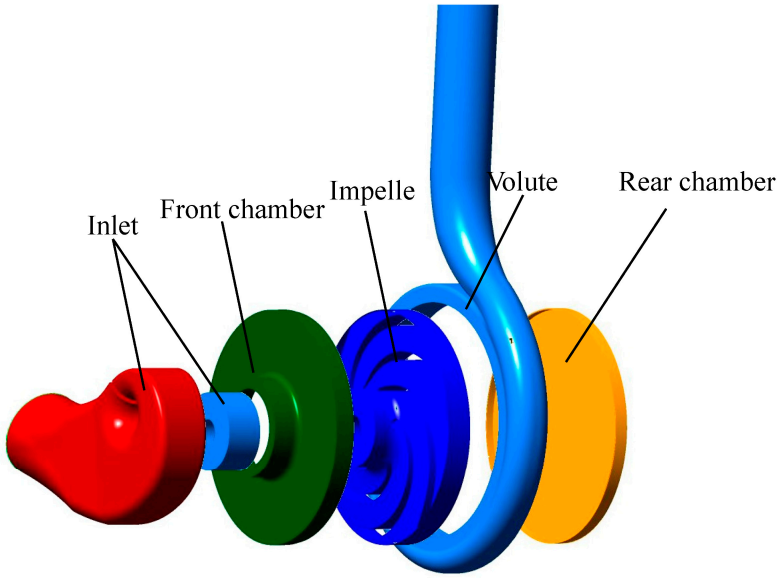

Figure 3. 3D model of the calculation domain.

3.2. Mesh Generation and Mesh Independence

Due to the use of full flow field calculation, the physical size at the gap of orifice is extremely small compared to the physical size of other water bodies; all calculation domains are divided by hexahedral structure meshes. The volute is stretched and combined with O-Block mesh. The spiral suction chamber domain (inlet domain) is divided by the whole block and combined with Y-Block. The impeller is only divided for a single flow channel, and wall boundary layer is achieved by controlling the distribution of nodes at the end of block edge. Then, perform a periodic array to obtain the mesh domain of entire impeller region. The meshing results are shown in Figure 4, and the mesh information of different computing domains is shown in Table 4. As we know, the minimum mesh quality and the minimum angle of grid are the guarantee of simulation accuracy. The minimum mesh quality is over 0.35 and the minimum angle of grid is over 20.7°, which meets the requirement of simulation.

The mesh independence verification has been conducted after mesh generation. The same topology has been applied to each domain, and the mesh number has been changed by adjusting the nodes of each topology line. The mesh quality is still controlled to meet the requirement of simulation. The y+ of each domain is less than 100. Figure 5 shows the pump head with different mesh elements. It shows that the pump head changes little when the mesh number is over 1.1 million elements. After

considering the computing resource and the simulation accuracy, the total grid about 1.2 million elements are selected to conduct the simulation.

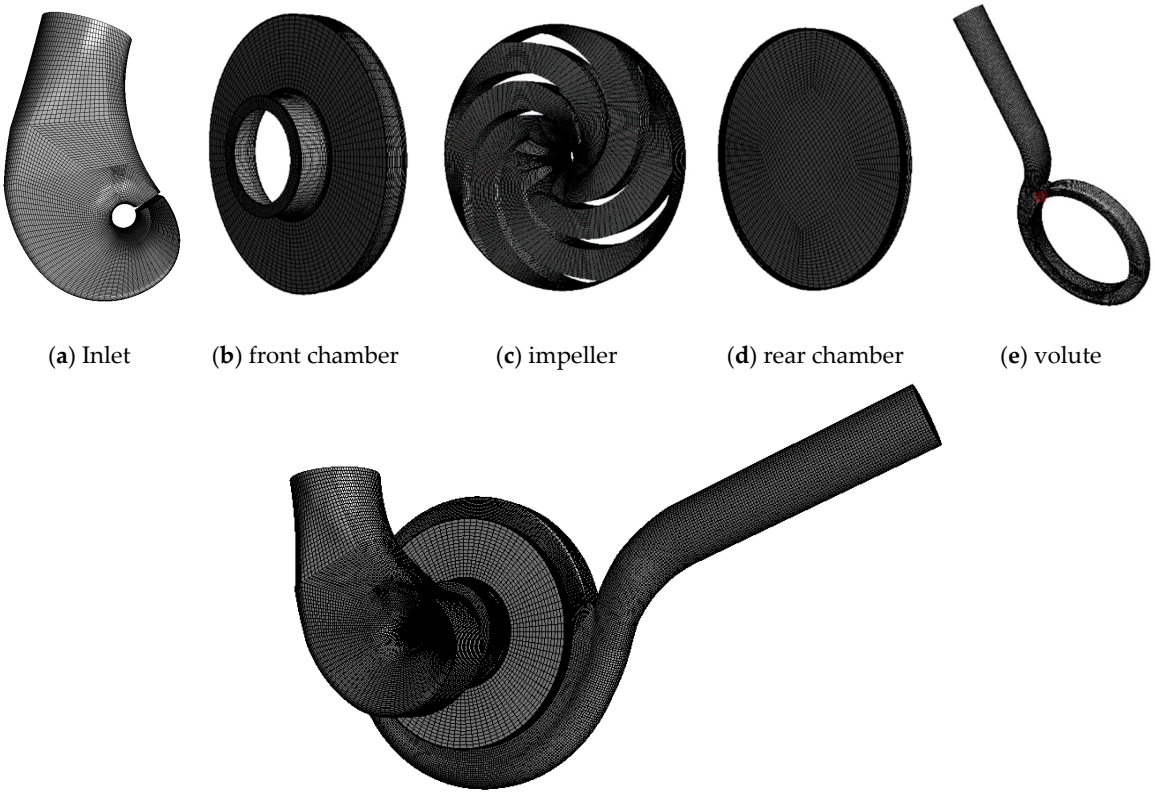

(**a**) Inlet (**b**) front chamber (**c**) impeller (**d**) rear chamber (**e**) volute

(**f**) Assembled mesh by each part

Figure 4. Structured mesh for the numerical domains.

Table 4. Mesh information of the numerical domain.

Computational Domains	Inlet	Front Chamber	Impeller	Rear Chamber	Volute
Quality	>0.35	>0.72	>0.4	>0.7	>0.55
Minimum Angle/°	>22.6	>54.3	>20.7	>41	>35.2

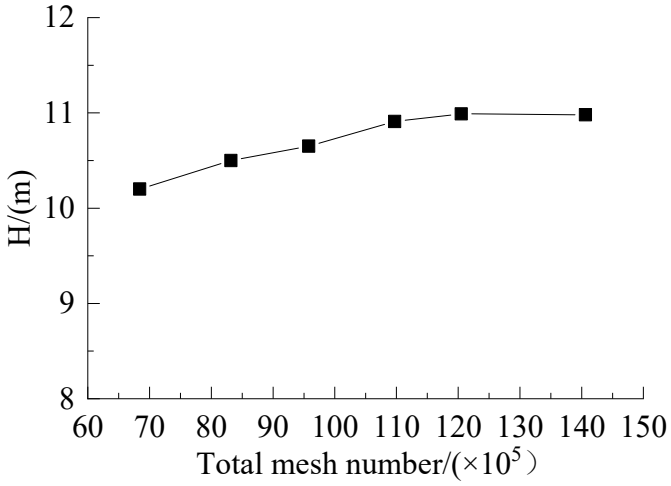

Figure 5. Pump head with different mesh number.

3.3. Selecting the Turbulence Model and Boundary Conditions

A universal turbulence model that is applicable for all flow problems has not yet been formulated; thus, scholars have selected different turbulence models for different turbulent flows. In this study, numerical calculations were performed with ANSYS CFX software, which provides a number of turbulence models. Therefore, five models, i.e., standard k-ε, RNG k-ε, k-ω, and SST k-ω, were selected, and their results were compared with each other. Table 5 shows the numerical results of the pump with different turbulent models under design flow condition of Qdes = 22 m^3/h. The relative pump head error from Number 1 to Number 4 is estimated as $(H_1 - H_d)/H_d$ = 5.55%, $(H_1 - H_d)/H_d$ = 3.36%, $(H_1 - H_d)/H_d$ = 6.45% and $(H_1 - H_d)/H_d$ = −0.09%, respectively. The head error is smallest when the standard k-ε model is selected. Therefore, this model was selected in this study. The finite volume method and the second-order windward scheme are applied to discrete the control equations. The inlet is set as velocity inlet and the outlet is set as opening. The standard wall function is chosen to calculate the near wall boundary, and the interfaces close to the impeller are set as Frozen Rotor. The convergence precision is set to 10^{-5}.

Table 5. Performance results with different turbulence models under design flow rate condition.

Number	Turbulence Models	H (m)
1	k-ω	11.61
2	RNG k-ε	11.37
3	SST k-ω	11.71
4	Standard k-ε	10.99

3.4. Identificatioin of High Efficiency Zones

Using the ANSYS CFX post processing tool CFX POST, the performance of the model pumps under the conditions of $0.6Q_{des}$, $0.8Q_{des}$, $1.0Q_{des}$, $1.2Q_{des}$, and $1.4Q_{des}$ are predicted respectively, and the performance parameters of the 11 different schemes are obtained. Figures 6 and 7 show the efficiency curves and head curves for 11 different impellers. To eliminate the influence of volute, the head and efficiency of impeller are calculated. The equations are as follows,

$$H_{impeller} = \frac{p_{2,impeller} - p_{1,impeller}}{\rho g} + \frac{v^2_{2,impeller} - v^2_{1,impeller}}{2g} \quad (6)$$

$$\eta_{impeller} = \frac{\rho g(Q/3600) \cdot H_{impeller}}{100P} \times 100\% \quad (7)$$

where $H_{impeller}$ represents the head of impeller, m; $\eta_{impeller}$ represents the efficiency of impeller, %; ρ represents the density of water at room temperature, ρ = 1000 kg/m^3; g represents the gravity, g = 9.8 m/s^2; $p_{1,impeller}$, $p_{2,impeller}$ represent the average circumferential pressure at impeller inlet section and impeller outlet section, respectively, Pa; $v_{1,impeller}$, $v_{2,impeller}$ represents the average circumferential velocity at impeller inlet section and impeller outlet section, m/s; and P represents the power of impeller, kW.

It can be seen from Figures 6 and 7 that either the head or efficiency of the impeller is higher than the pump because there is much more energy expenditure in volute and the influence of volute will discuss in the following section. Moreover, the head or efficiency of each scheme shows a large difference from large flow conditions to small flow conditions. The Impeller 1, Impeller 7, and Impeller 8 are the repeatability tests of center point and the energy performance values of three schemes are basically the same, indicating the stability of test environment. The efficiency and head distribution of other schemes are various at designed flow rate condition. For instance, the highest efficiency occurs at Impeller 2 and the value is about 83.02% while the lowest efficiency occurs at Impeller 4 and the value 79.45%. The highest head occurs at Impeller 9 and the value is 16.86, while the lowest head occurs at

Impeller 2 and the value 13.86. It indicates that the geometry of impeller is significant to the energy characteristics of pump. Thus, it is useful to change the geometry parameters of pump to improve the efficiency.

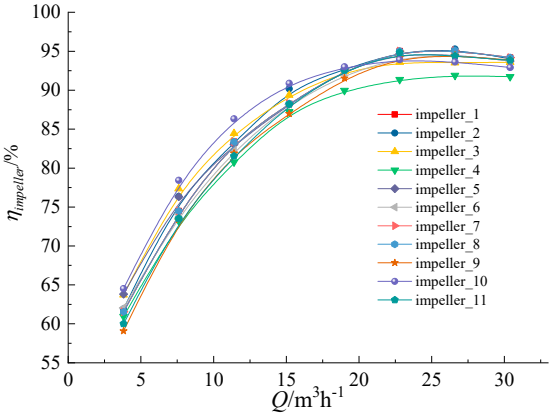

Figure 6. Efficiency curves of impeller under different schemes.

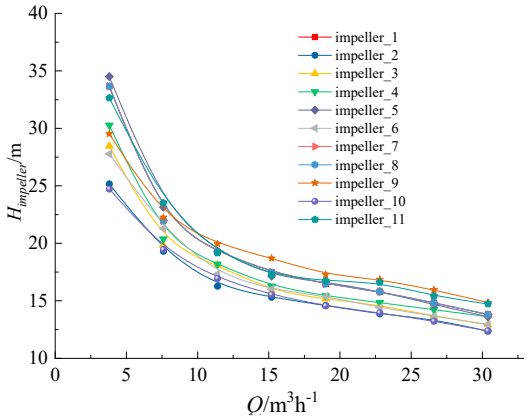

Figure 7. Head curves of impeller under different schemes.

4. Optimal Design of Impeller Based on FED

4.1. Influence of Experimental Factor

The energy characteristics prediction results show that the efficiency of 11 schemes is significantly different under large flow conditions and small flow conditions. Considering the limitation of numerical calculation resources and the actual operating characteristics of WECP, the operating conditions of $0.6Q_{des}$, $0.8Q_{des}$, $1.0Q_{des}$, and $1.4Q_{des}$ are selected as the operating conditions to optimize within the full range of flow rate conditions. The effects of various factors on impeller efficiency under these conditions are analyzed to make the efficiency curve gentler and the high efficiency region wider.

Minitab software is used to analyze the experimental data. All the main and two-order interaction effects are included in the model, including blade outlet width (A), blade outlet angle (B), blade wrap angle (C), and their interaction effects, like the blade outlet width multiply by the blade outlet angle (AB), blade outlet width multiply by the blade angle (AC), blade outlet angle multiply by the blade outlet angle (BC). The interaction above three orders is not considered. Figure 8 is Pareto diagram of the efficiency of impeller parameters.

It can be seen from Figure 8a that the A and B of impeller parameters have a significant influence on the efficiency at $0.6Q_{des}$. According to the intensity of influence, the A is higher than the B. Among the three main effects affecting the efficiency at $0.6Q_{des}$, the A and B are more significant, but the C

is not significant. The three 2-factor horizontal interaction effects have no significant effects on the efficiency at $0.6Q_{des}$. It can be seen from Figure 8b that the A, B, and C of three main effects have a significant effect on the efficiency of $0.8Q_{des}$. Among the three 2-factor horizontal interaction effects, AB has a greater impact on the efficiency of $0.8Q_{des}$ operating point. The effect of BC and AC on the efficiency under $0.8Q_{des}$ is not obvious, and it should be removed when the model is improved. It can be seen from Figure 8c that the impeller parameters which have a significant influence on the efficiency of $1.0Q_{des}$, including A and AB. As can be seen from the figure, A and AB have a greater impact on efficiency. It can be seen from Figure 8d that all the effects listed in the model have a significant effect on the efficiency of $1.4Q_{des}$. According to the intensity of influence, it can be arranged as A, AC, C, B, AB, and BC.

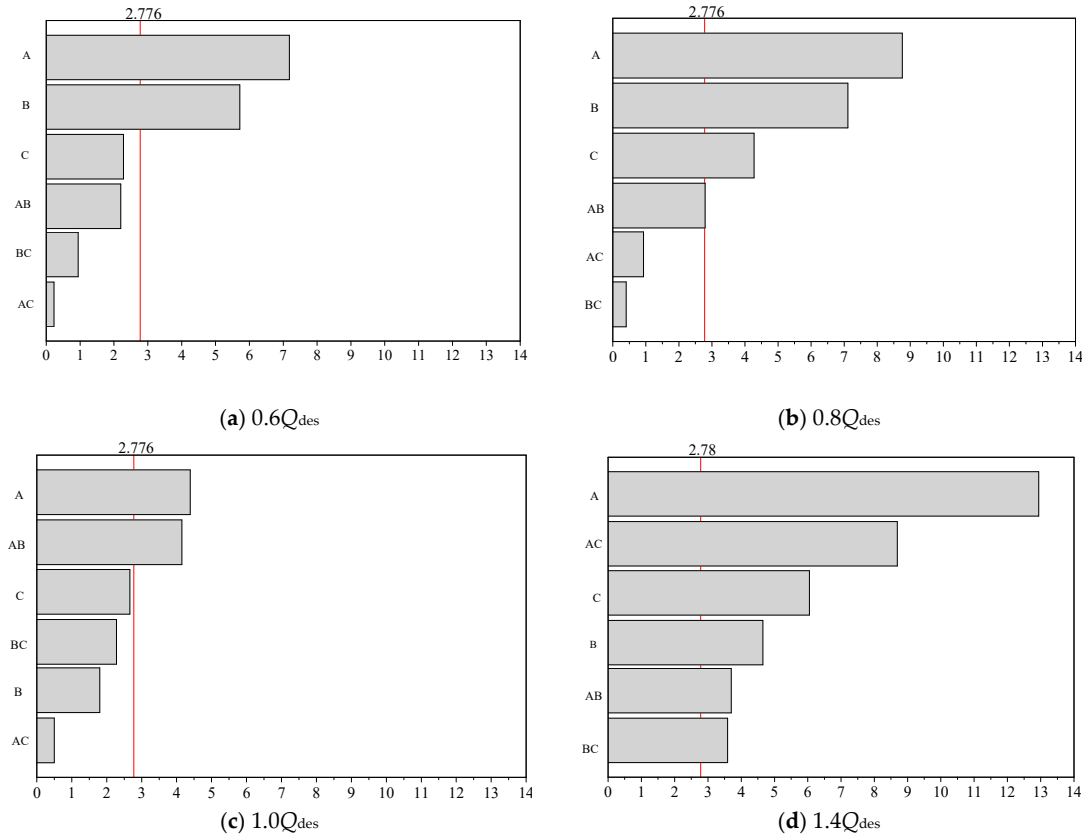

Figure 8. Pareto diagram of efficiency under different operation conditions.

The main effect diagram of efficiency is shown in Figure 9. As can be seen from Figure 9a, the regression lines of blade outlet width and the blade outlet angle are steeper. That is, the two have a greater influence on the efficiency of $0.6Q_{des}$ operating point. At the same time, the blade wrap angle also has a certain effect on the efficiency. However, the regression line is not as steep as the regression angle of blade outlet width and blade outlet angle: the line is relatively flat. This also confirms that in the Pareto diagram, although the C has not been selected as a significant effect, it is also very close to the critical value. Therefore, it also has a certain impact on efficiency. At the same time, as A and B increase from a low level to a high level, the efficiency decreases under $0.6Q_{des}$ operating point. It can be roughly seen that in order to maximize the efficiency of $0.6Q_{des}$ operating point, the A and B can be simultaneously lowered.

It can be seen from Figure 9b that the regression lines of the A, B, and C are steep. That is, the three factors have an obvious effect on the efficiency of $0.8Q_{des}$ operating point. When A increases from 19 mm to 23 mm or the B increases from 16° to 22°, the efficiency of $0.8Q_{des}$ operating point shows a downward trend. However, when C increases from a low level to a high level, the efficiency

increases at $0.8Q_{des}$. It can be seen from Figure 9c that the A regression line is steep, namely, the A has the most obvious effect on the efficiency of $1.0Q_{des}$ operating point. As the A increases from a low level to a high level, the efficiency of $1.0Q_{des}$ operating point decreases. At the same time, the two factors of B and C also have a certain effect on efficiency. However, the regression line is not as steep as the regression angle of blade outlet width, and it is relatively flat. This also confirms that in the Pareto diagram, the B and C have not been selected for significant effects, but they are also very close to the critical value, so the two have a certain effect on the efficiency. It can be seen from Figure 9d that the regression lines of the A, B, and C are all steep, namely, the three factors have obvious influence on the efficiency of $1.4Q_{des}$ operating point. When the A increases from 19 mm to 23 mm, the efficiency of $1.4Q_{des}$ operating point increases, whereas the B increases from 16° to 22° or the C increases from 150° to 170°, the efficiency of $1.4Q_{des}$ operating point decreases.

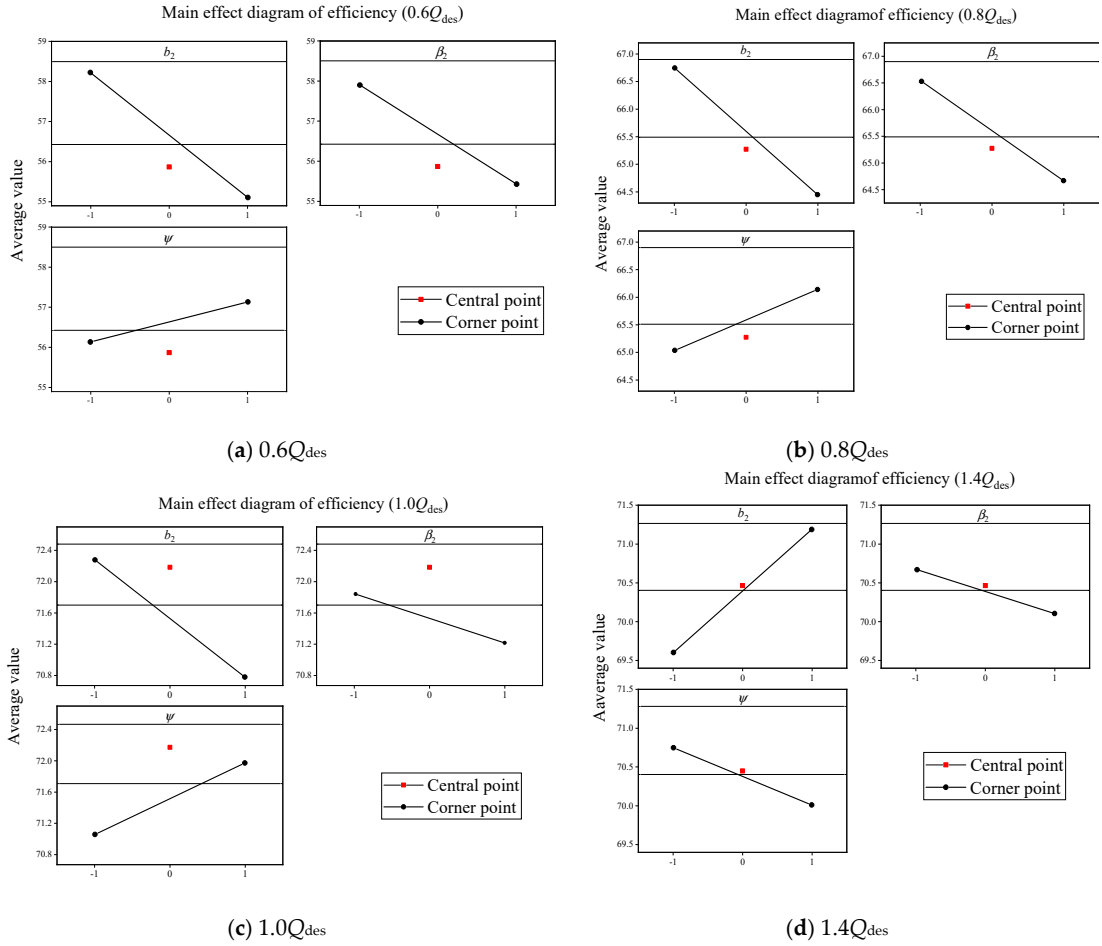

(**a**) $0.6Q_{des}$ (**b**) $0.8Q_{des}$

(**c**) $1.0Q_{des}$ (**d**) $1.4Q_{des}$

Figure 9. Main effects diagram of different operation conditions.

The interaction effects could reveal the difference in the amount of response between various levels of a factor changes with the different levels of other factors. When there are two or more independent variables in an experimental study, the main effects are not sufficient to find the non-independent effects of several factors. Therefore, the interaction parameters and the interaction effect diagram could evaluate the changes of a factor at different levels which depends on other factors. In this study, the interaction effects show the relationship of different parameters. Figure 10 shows the interaction diagram of efficiency. It can be seen from Figure 10a that the interaction line of BC is almost parallel to the line of AC, which explains that the interaction between these two groups has no significant effect on the efficiency of $0.6Q_{des}$ operating point. The interaction line of AB is not parallel to the other two groups, but the cross trend is not obvious. It can also be seen from the Pareto diagram that, although

AB has not been selected as a significant effect, the t value in t-test is also very close to the critical line, so it also has a certain impact on efficiency. It can be seen from Figure 10b that the interaction line of AB is obviously not parallel, indicating that the interaction between the two is obvious. Two sets of interaction lines of BC and AC are almost parallel, showing that it has no significant effect on the efficiency of $0.8Q_{des}$ operating point. It can be seen from Figure 10c that the interaction line of AB produces crossover and even form a reverse interaction (when the blade outlet width is at a low level, the efficiency decreases as the blade outlet angle increases, and when the blade outlet width is at a high level, the efficiency increases as the blade outlet angle increases). Similarly, for the BC, the interaction line is not parallel, but not so obvious compared with the interaction line of AB. This also confirms that in the Pareto diagram, BC has not been selected as a significant effect. However, the t value in the t-test is also very close to the critical value, so it also has a certain impact on efficiency. The interaction line of AC is almost parallel, which has no significant effect on $1.0Q_{des}$ operating point efficiency. It can be seen from Figure 10d that the three sets of interaction lines are not parallel, indicating that the interaction is obvious. Among them, when the blade wrap angle is taken low, the efficiency is not obviously improved as the blade outlet width increases. However, when the blade wrap angle is high, the efficiency increases significantly as the blade outlet width increases. This shows that the AC interaction has a greater impact on efficiency, which is also consistent with the Pareto diagram, and the AC effect is second only to the main effect of A.

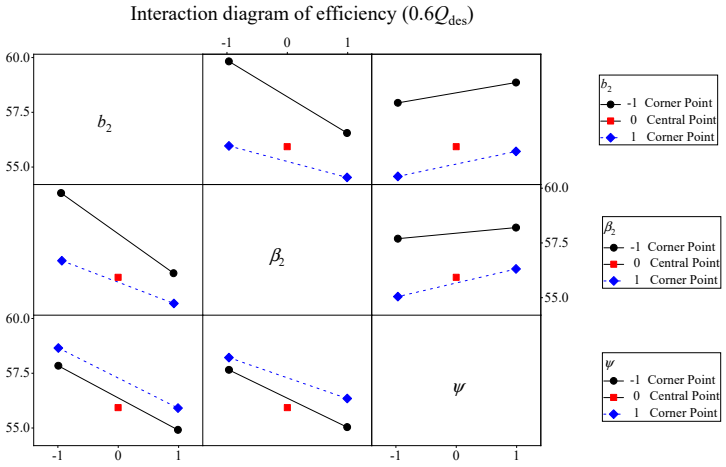

(**a**)

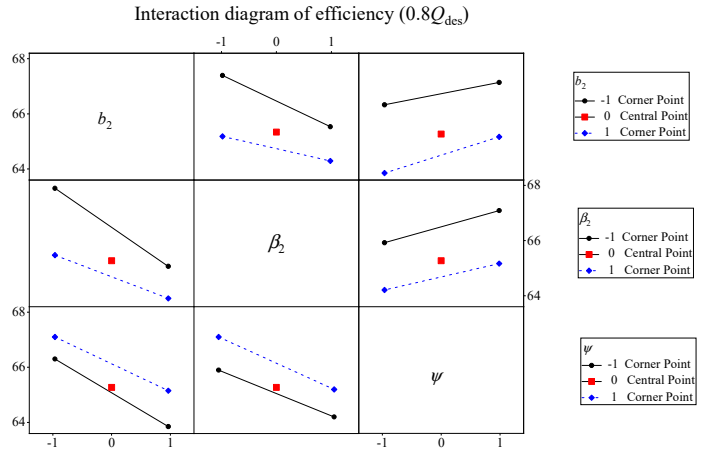

(**b**)

Figure 10. *Cont.*

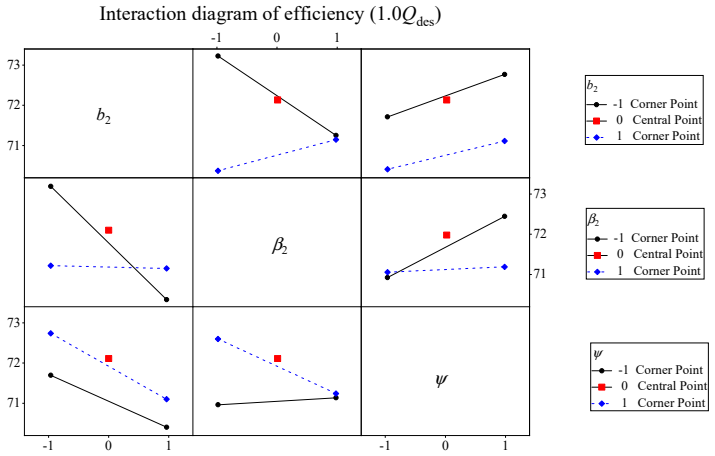

(**c**)

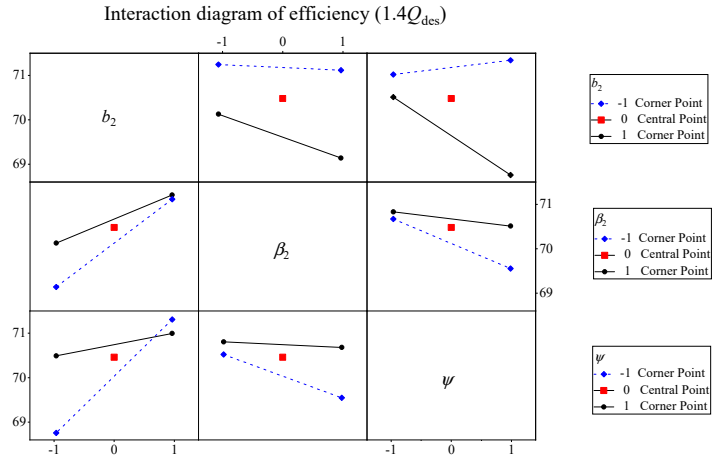

(**d**)

Figure 10. Interaction effect diagram of different flow rate point: (**a**) Interaction effect diagram of 0.6Q_{des}. (**b**) Interaction effect diagram of 0.8Q_{des}. (**c**) Interaction effect diagram of 1.0Q_{des}. (**d**) Interaction effect diagram of 1.4Q_{des}.

4.2. Geometric Parameter of Optimization Model

Based on variance analysis and residual diagnosis, the regression model of efficiency and impeller parameters under different working operations is obtained:

$$0.6Q_{des}\text{: } Y = 56.422 - 1.52A - 1.207B \tag{8}$$

$$0.8Q_{des}\text{: } Y = 65.49 - 1.104A - 0.896B + 0.538C + 0.317AB \tag{9}$$

$$1.0Q_{des}\text{: } Y = 71.6745 - 0.7412A - 0.3037B + 0.7012AB \tag{10}$$

$$1.4Q_{des}\text{: } Y = 70.4436 + 0.775A - 0.28B - 0.3625C + 0.2225AB + 0.52AC - 0.215BC \tag{11}$$

According to the influence of impeller geometric parameters on efficiency, the calculation of the blade outlet width b_2, the blade outlet angle β_2, and the blade wrap angle ψ in Equations (8)–(11) can be performed. In fact, according to the specific requirements of optimization objectives, the target of different working operations is set as "hope big features", namely, Y should be larger at each operating point. Referring to the relevant literature [29], and according to the engineering experience, the weights of the four operating points of 0.6Q_{des}, 0.8Q_{des}, 1.0Q_{des}, 1.4Q_{des}, are 0.221, 0.286, 0.46, and 0.319, respectively. Afterwards, the response optimization results of blade outlet width b_2, the blade outlet

angle β_2, and the blade wrap angle ψ is −0.4902, 0.3307, and 0.5, respectively, which is automatically given by Minitab software. Therefore, a simple interpolation operation could be applied to calculate the geometry parameters. After optimization, the optimal parameters of the impeller according to the target are obtained, where b_2 = 20.02 mm, β_2 = 20°, ψ = 165°. The geometric parameters of the impeller before and after optimization are shown in Table 6.

Table 6. Parameter contrast.

Parameter	Original Impeller	Optimized Impeller
b_2/mm	21	20.02
β_2/°	19	20
ψ/°	150	165

4.3. Energy Performance of the Optimization Model

According to the optimized parameters of the impeller, a new hydraulic diagram of impeller is redrawn with the help of PCAD software. The 3D modeling of impeller was built and the whole flow domain is obtained. The whole fluid domains with optimized impeller are divided into structured meshes and then calculated. The ANSYS CFX is used to calculate the full flow field of the pump before and after optimization. The comparison of the energy characteristic curves of the original impeller and optimized impeller are shown in Figure 11. It can be seen from the figure that the head of the optimized impeller is slightly higher than that of the original impeller from $0.2Q_{des}$ to $1.4Q_{des}$, but the efficiency drops a little. For example, at the designed flow rate condition, the head of original impeller is 10.99, and it is improved to 11.99 after optimization, which is 8.34% higher than the original impeller. However, the expansion of high efficiency region may cost some efficiency of pump, though it is acceptable. If the critical line is set in the efficiency curve, which is 90% of the highest efficiency point, the region of optimized impeller is wider than the original one. Also, from the perspective of weighted average efficiency, the weighted average efficiency of optimized impeller under the condition of $0.6Q_{des}$, $0.8Q_{des}$, $1.0Q_{des}$, $1.2Q_{des}$, and $1.4Q_{des}$ is 69.49%, which is 2.55% higher than the original impeller. It can be seen that the optimized impeller high efficiency region is obviously widened, the impeller efficiency curve is gentle, and the overall efficiency of the WECP is effectively improved, and the optimization objective is achieved.

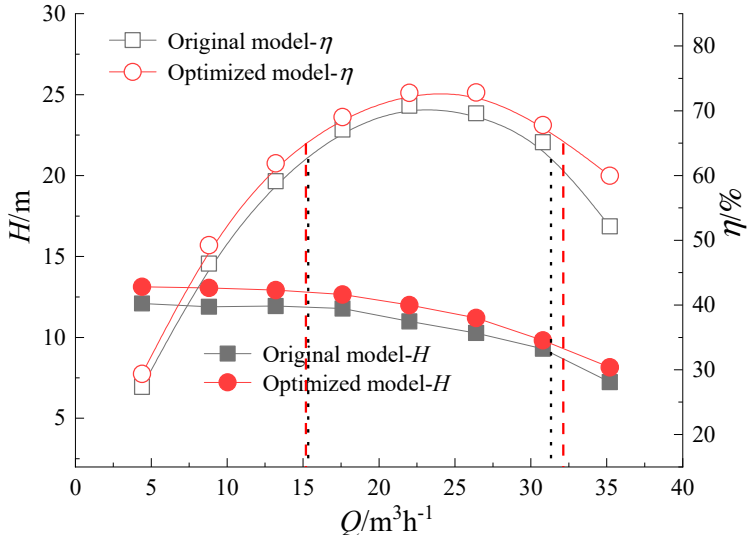

Figure 11. Performance curves of optimized impeller and original impeller.

5. Matching Features between Impeller and Volute

After optimization, the high efficiency region of impeller is obviously widened, which improves the overall efficiency of centrifugal pump and achieves the optimization goal. However, in the experimental design, due to the consideration of test cost, only three impeller parameters, namely, the blade outlet width b_2, the blade outlet angle β_2, and the blade wrap ψ angle, are selected as the independent variables while the geometric parameters of volute are not considered at that stage. However, the impeller and volute are the main overcurrent components of centrifugal pump. Thus, the combination of them also affects the pump performance and there is an optimal matching relationship [30]. To further explore ways to improve the performance index of WECP, and then improve the efficiency of pump unit and achieve energy saving, based on the optimized impeller, by changing the angle of volute tongue angle, the energy characteristics and internal flow of centrifugal pump are studied. The impact provides a theoretical basis for the performance improvement of WECPs.

5.1. Optimum Proposal

Under the circumstance of constant structure parameters of centrifugal impeller, three types of volute are designed with the tongue angle of 23°, 28°, and 33°. The 3D model of different volute domain is shown in Figure 12. The same numerical method is adopted to calculate the whole flow passage considering the clearance in pump cavity. Hexahedral mesh generation method is adopted for all computation areas. After stretching and merging with 3/4 O-Block, the whole O-Block mesh operation is carried out. The same boundary conditions are set in three cases. The inlet boundary is set as velocity inlet and the outlet boundary is set as opening. No-slip boundary condition is applied to all the walls. The standard wall function is used to deal with the flow near the wall region. The dynamic and static interface is set as Frozen Rotor. The computational convergence accuracy is set to 10^{-5}.

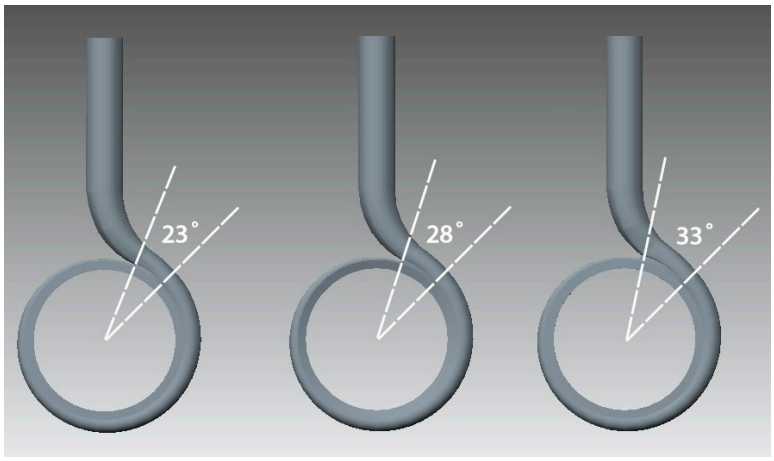

Figure 12. 3D model of different volute.

5.2. Selection of the Volute

5.2.1. Prediction of Energy Characteristics Results

Through numerical simulation, the head curves and efficiency curves of three different types of WECPs are obtained, as shown in Figure 13. Note that the head and efficiency of WECPs are obtained in this section rather than the partial head and efficiency of impeller, due to the influence of volute is considered. It can be seen from the figure that when the angle of the tongue is increased from 23° to 28°, there is little difference in heads under small flow condition. Under high flow conditions, as the flow rate increases, the pump head drops sharply when the tongue is placed at an angle of 23°, and the head curve is flat when the tongue angle is 28°. When the tongue angle changes from 28° to 33°, the

head decreases slightly under small flow conditions. After the $1.0Q_{des}$ operating point, as the flow rate increases, the pump head drops more significantly when the tongue angle is 28°. At the $1.6Q_{des}$ operating point, the pump head with the tongue angle of 28° and 33° is 7.94 m and 8.79 m, respectively, with a difference of 0.85 m.

When the tongue angle increases from 23° to 28°, the efficiency does not change much under small flow conditions. Under large flow conditions, when the tongue angle is placed at 28°, the efficiency is significantly higher than that at 23°. When the tongue angle is 28° and 33°, both of the pumps' efficiency does not much different before $1.2Q_{des}$ working condition, but after $1.2Q_{des}$ working condition, with the increase of flow rate, the WECP with the tongue angle of 33° has a more gradual efficiency curve and wider high efficiency zone. The results show that with the increase of tongue angle, the head of WECP has been improved, the high efficiency range of hydraulic efficiency has been widened as well, and the highest efficiency point moves toward the large flow direction.

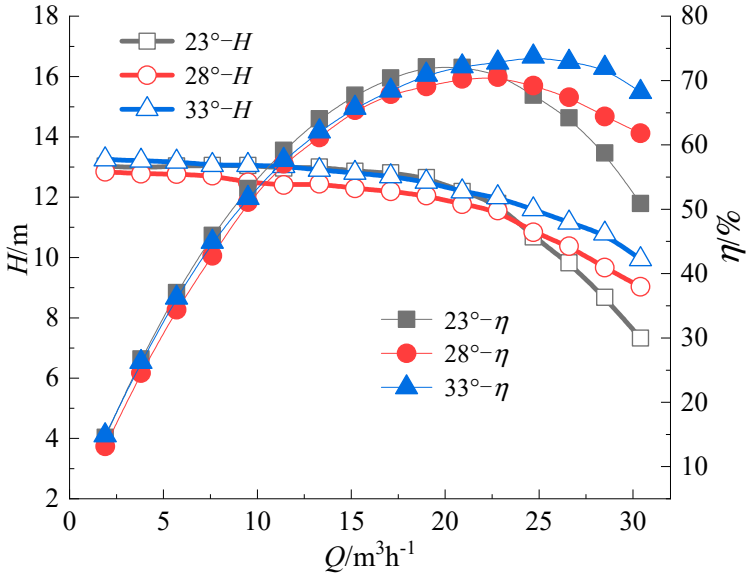

Figure 13. Performance curves with different volutes.

5.2.2. Analysis of Inner Flow

The postprocessing tools CFX-POST provided by ANSYS CFX are utilized to acquire the flow fields of WECP with different tongue angle volutes. The velocity distribution of WECP with different tongue angles on the symmetric surface of volute under design condition is shown in Figure 14. It can be seen from the diagram that the velocity distribution trend on the symmetrical surface of centrifugal pump volutes with different tongue angles are basically the same. The velocity distribution in flow channel near the tongue is not uniform, and there is a clear velocity gradient. Because of the difference of tongue angle, the flow characteristics in the downstream diffuser have been affected greatly. With the tongue angle of 23°, the low speed zone moves backward toward the outlet pipe, and the range and intensity of the low speed zone decrease obviously. However, with the angle of 33°, the influence of tongue angle on the internal flow of centrifugal pump is further weakened. The low velocity area in the diffuser is not obvious and the flow inside the impeller is even more uniform.

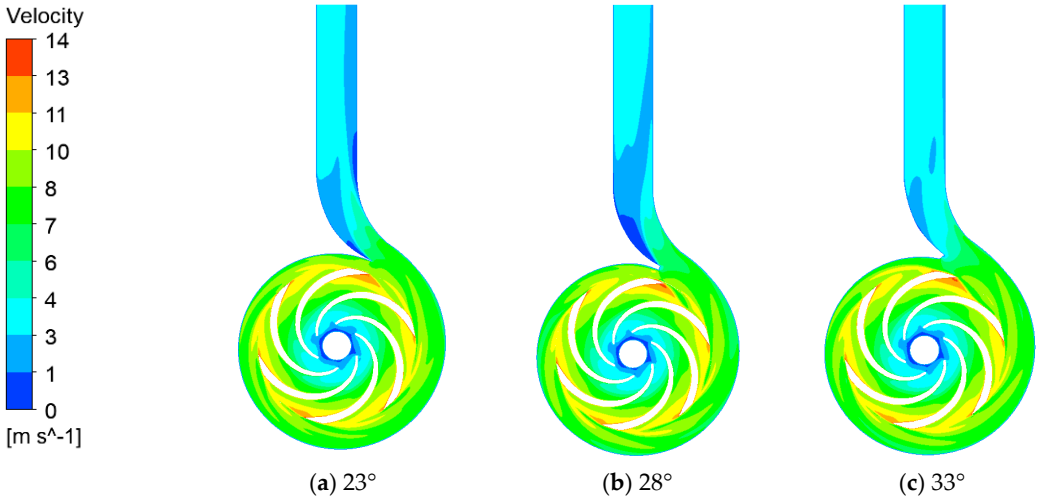

Figure 14. Velocity distribution on volute cross section under design flow rate condition with different volutes.

The pressure distribution of WECP with different tongue angles on the symmetric surface of volute under design condition is shown in Figure 15. The great impact of tongue angle on the pressure distribution at the outlet of volute can be seen in the diagram. With the increase of tongue, the pressure increases at the outlet of volute, which indicates more kinetic energy of fluid are converted to the potential energy. Furthermore, the pressure distribution is more uniform at the outlet of volute when the volute tongue angle is 33°. This shows the better hydraulic feature of volute. Combining with the torque at different tongue angle in Table 7, the torque with different tongue angles have little difference, and it is moderate when the tongue angle is 33°. Those features show the better characteristics of 33° volute.

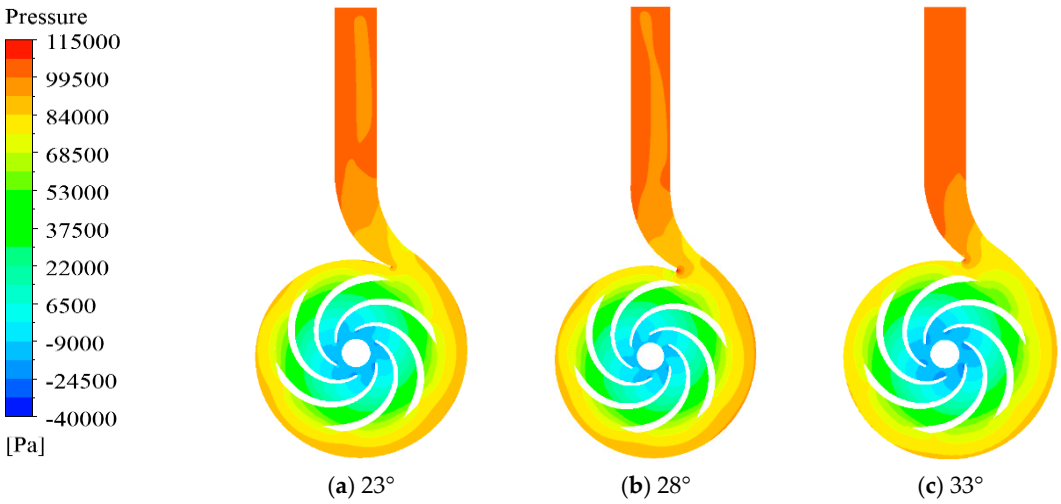

Figure 15. Pressure distribution on volute cross section under design flow rate condition with different volutes.

Table 7. Torque of impeller with different volutes.

Tongue Angle/°	23	28	33
Torque/N·m	6.19	6.11	6.15

Four radial cross sections (Section I (0°), Section III (90°), Section V (180°), and Section VII (270°)) are selected to analyze the internal flow in volute, and the positions of different cross sections are shown in Figure 16. The velocity and the vector in those cross sections are shown in Figure 17, respectively. It

can be seen from Figure 17 that the flow inside the volute is unstable, there are various kinds of vortices on each section, and the flow field distribution is complicated. In the section I (0°), the placement of tongue angle has a great influence on the secondary flow velocity distribution. The flow of this section has been affected by the flow of tongue gap, and the mainstream speed is larger. The flow in first section of 33° volute is more stable than the other two types of volute. Close to the tongue area, the vortex has not been formed fully in 0° radial section of 33° volute. At the same time, as the tongue angle reduces, the intensity of vortex is more and more obvious in 0° radial section of 23° volute. A pair of oppositely directed vortices was formed in the radial section and it is clearly visible. In the Section III (90°), more and more fluids enter in the volute. The three types of volutes have opposite vortices in 90° section and exhibit a "right strong left weak" condition. When the fluid reaches section V from III, the fluid entering in the volute further increases. As the impeller outlet flow velocity distribution along the impeller outlet width is not uniform, the fluid entering in the volute is deflected because of this influence. For the 23° volute, the right vortex is not obvious, and the left vortex intensity becomes larger, affecting the velocity distribution of entire section. Although the right vortex still exists in this section of 28° volute, its strength has been weakened and its intensity is lower than the left vortex. The influence of the uneven distribution of impeller outlet velocity of 33° volute is relatively unobvious, and the strength of the left and right vortices is equal. In VII section, the left vortex is still intensive, and the right vortex gradually grows. When the tongue angle is 23°, the intensity of left vortex is slightly higher than the right vortex, which is much different than the other sections. Further, the right vortex in section VII of 28° volute develops much and its strength is nearly equal to the left vortex. When the volute tongue angle grows to 33°, even though the influence range of vortex increases, the left and right vortexes remain basically symmetrical. In summary, the flow fields in volute with different tongue angles present a complex flow state, and the flow advances in the direction of liquid flow almost in the form of a vortex. Along the direction of the liquid flow, as the angle increases, those vortexes also evolve and separate. The placement of tongue angle has a great influence on the vortex flow of each section. As the tongue angle increases, the influence of vortexes on each section becomes weaker, and the flow fields are more stable, which is consistent with the analysis of velocity distribution trend.

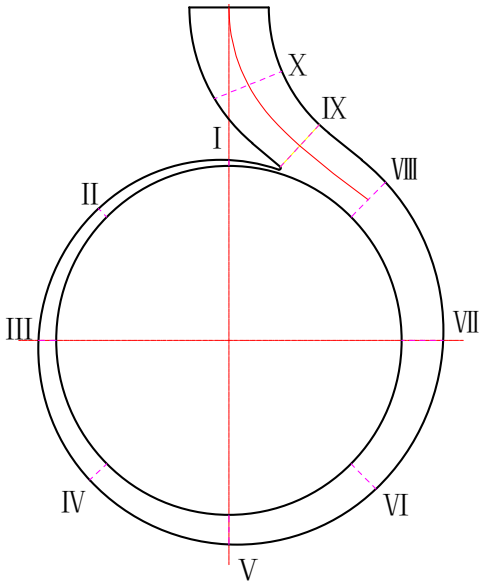

Figure 16. The positions of the cross sections.

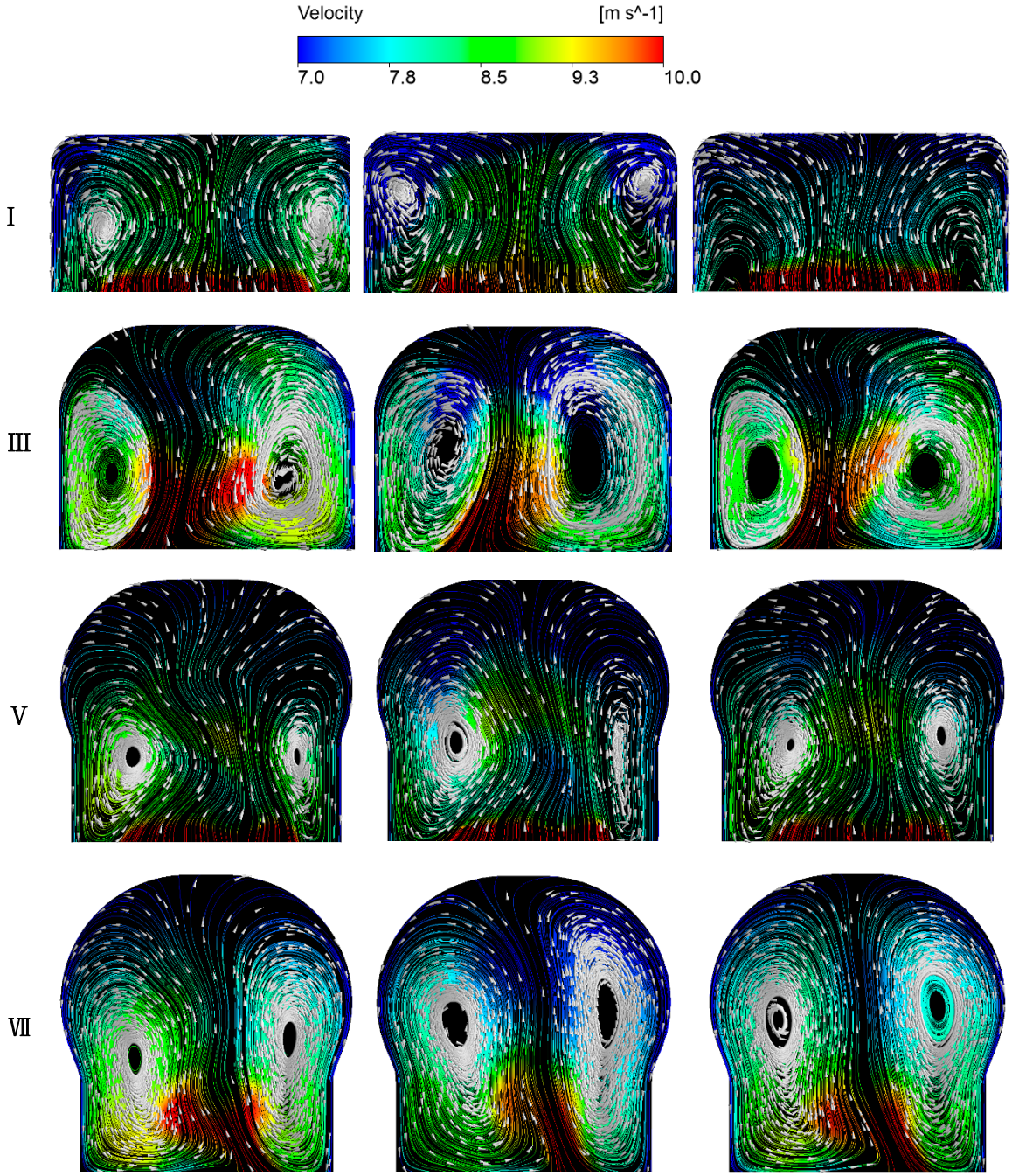

(**a**) 23° (**b**) 28° (**c**) 33°

Figure 17. Vector distribution of four radial cross sections under design flow rate condition.

The turbulent kinetic energy distribution inside WECP with different tongue angles under design condition is shown in Figure 18. As can be seen from the diagram, the turbulent kinetic energy distribution inside the spiral water suction chamber, the impeller, and the front and back pump cavity is basically the same, but the turbulent kinetic energy of first section with 23° volute is obviously larger than the other two types of volute. The distribution of turbulent kinetic energy inside the volute cross section with the volute tongue angle of 33° is the most uniform with the tongue angle of 33°. Through the analysis of the internal flow fields of WECP, it is known that the proper increase of tongue angle can effectively improve the internal flow of WECPs.

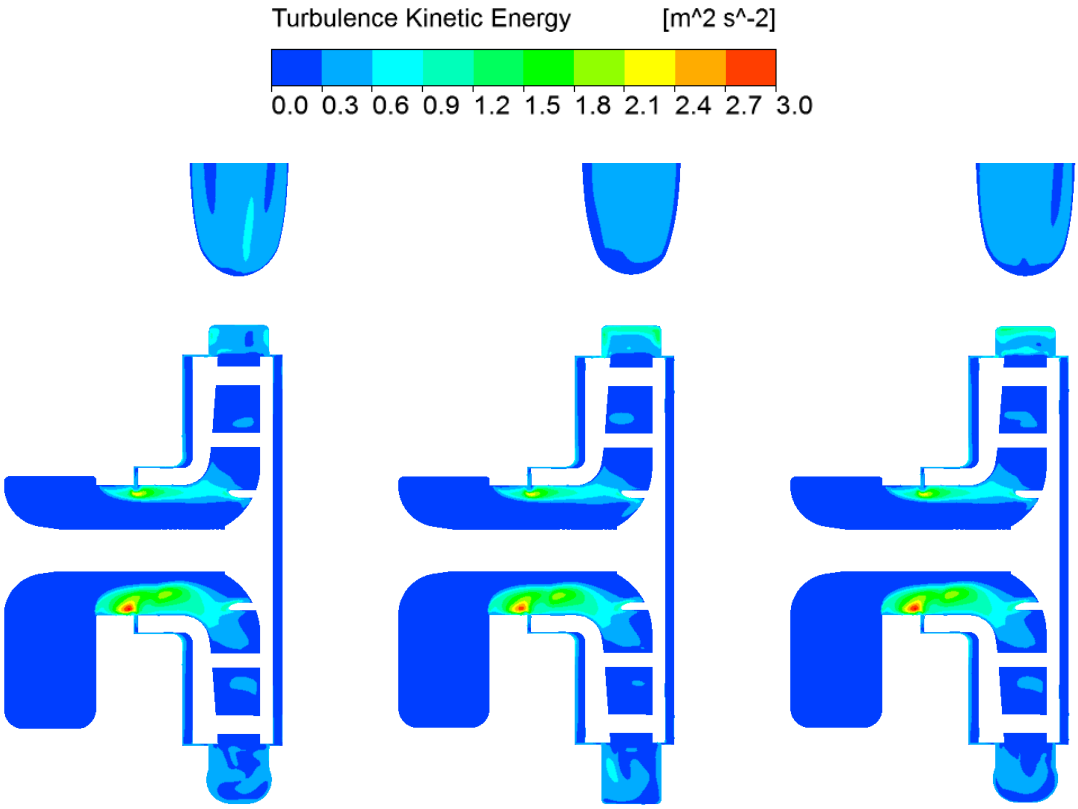

(**a**) 23° (**b**) 28° (**c**) 33°

Figure 18. Distribution of turbulent kinetic energy under design condition with different tongue angles.

6. Verification of Energy Performance of Optimized Model

6.1. Testing Pump and Facilities

The impeller and volute are made of fully transparent plexiglass. The physical model of impeller and volute is shown in Figure 19. To verify the accuracy of numerical simulation, the test bed has been established for testing energy characteristic of WECP as shown in Figure 20. Its test bed reaches 1 level required precision. The external characteristic test has been carried out on the prototype model of WECP with the tongue angle of 33°.

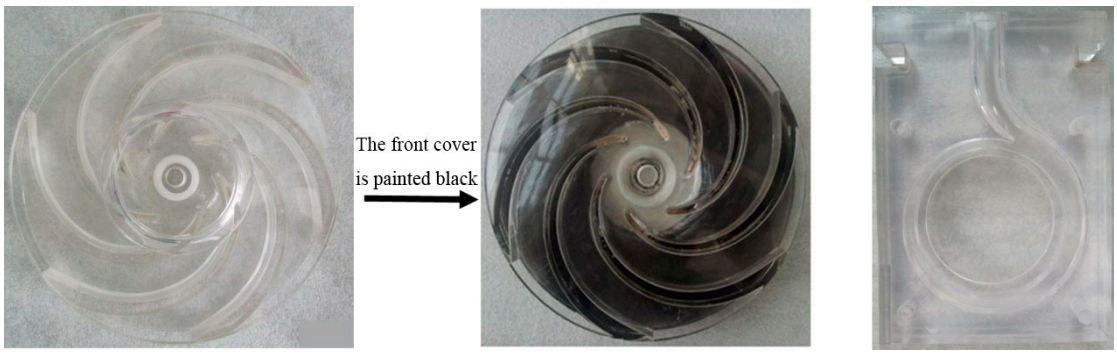

Figure 19. Model.

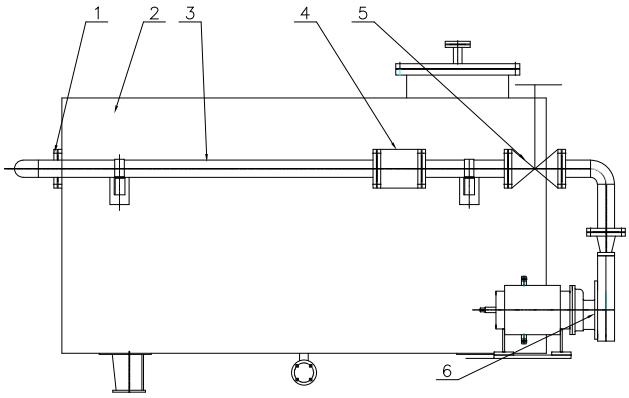

Figure 20. Test bed. 1. Pipeline export. 2. Water tank. 3. Pipeline. 4. Electromagnetic flowmeter. 5. Discharge valve. 6. Test pump.

6.2. Analysis of Energy Characteristic Results

During the test of energy characteristics, the reliability can be guaranteed by collecting the data thrice under each flow rate condition and the comparison between repeated results are is shown in Figure 21. According to the repeatability test results, the low difference in head and efficiency of three repeated tests indicates that the test environment is stable and the reliability of test bed and test system is good.

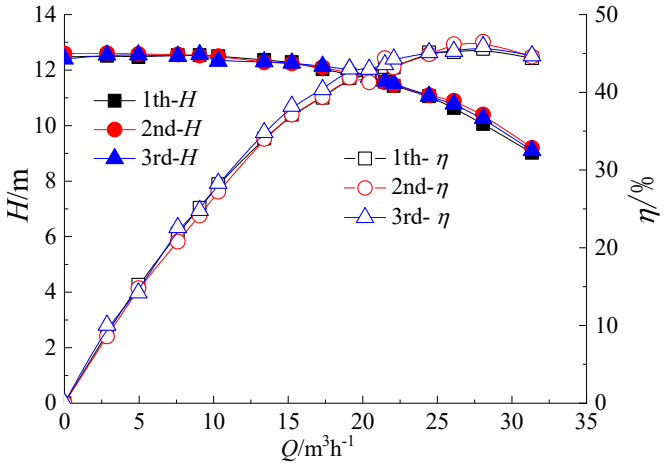

Figure 21. Performance curves of repetitive testing.

Comparing experimental and CFD results, the external characteristic curves are plotted respectively, as shown in Figure 22. Even though the pump efficiency of WECP is calculated by the same equation, the actual value of efficiency is impossible to be the same because of the complexity of boundary in reality. In engineering fields, the difference is acceptable as long as the error is within a reasonable range. Therefore, the difference of head is particularly discussed in this paper. It can be seen from the figure that the pump head of numerical calculation is close to the experiment results and the calculated head is slightly higher than the test. At the design point, the calculation head is 11.89 m and the test head is 11.28 m, which indicates the pump head is predicted to be about 5.4% higher than the test value. However, under the small flow condition, the test value is close to the calculated value. Furthermore, there is a certain difference under large flow condition. The average head of numerical calculation is higher than the experimental value of ~5%. Excluding some small influence factors, two main reasons may account for this phenomenon. On one hand, the inlet flow is simplified into uniform flow in numerical calculation, which is different from the actual situation. On the other

hand, the head will be reduced by cavitation occurring under large flow rate condition, which is not considered in numerical calculation. On the whole, the numerical simulation head is basically same as the experimental measurement head. The results show that the numerical calculation method adopted in this paper is accurate and feasible as a means of experimental implementation.

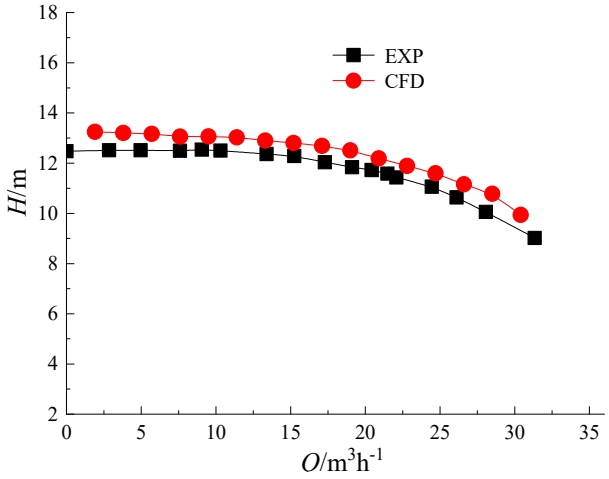

Figure 22. Comparison between experiment and simulation.

7. Conclusions

In this paper, based on FED and CFD methods, the optimal design of WECP has been successfully conducted. Eleven schemes of experiments were designed to research the effect of experimental factors, including blade outlet width b_2, blade outlet angle β_2, and blade wrap angle ψ. A mathematical model related to the efficiency of different working conditions and the main geometric parameters of impeller was established. Meanwhile, the matching characteristics of impeller and volute were numerically studied. The results of the analysis are as follows.

(1) The relationship model between impeller geometric parameters and efficiency can be established by FED-CFD method. The mathematical model contains the main effects and interaction effects of impeller geometric parameters on pump efficiency. Blade outlet width dominates the main effect and interaction term. The interaction between the blade outlet width and the blade wrap angle or the interaction between blade outlet width and the blade outlet angle has a significant effect on the efficiency of large flow operating point. However, the effect of interaction on efficiency in small flow conditions can be ignored.

(2) The matching of impeller and the volute is essential to improve the overall efficiency. Under large flow conditions, the volute tongue angle is positively correlated with head and efficiency. As the tongue angle is increased, the head of centrifugal pump is increased, the efficient range of hydraulic efficiency is widened, and the highest efficiency point is moved toward the large flow direction.

(3) Implement the optimal design of WECP by FED-CFD method. After optimization, the head curve of impeller is relatively flat, the efficiency is at a high level, and the high efficiency region is widened. The weighted average efficiency of four operating points increases by 2.55%, which improves the overall efficiency of WECP. Through the experimental verification, the established optimization design method for combination of FED and CFD is reliable and effective, and can be applied to the optimization design of multi-condition centrifugal pump.

Author Contributions: Methodology and project administration, W.L.; writing—original draft preparation and review and editing, L.J.; review and editing, W.S., L.Z., H.C. and R.K.A. All authors have read and agreed to the published version of the manuscript.

Funding: The work was sponsored by the National Key R&D Program Project (No. 2017YFC0403703), National Natural Science Foundation of China (Nos. 51679111, 51409127 and 51579118), PAPD, Key R&D Program Project in Jiangsu Province (BE2016319, BE2017126), Natural Science Foundation of Jiangsu Province (Nos. BK20161472, BK20160521), Science and Technology Support Program of Changzhou (No. CE20162004), Key R&D Program Project of Zhenjiang (No. SH2017049), and Scientific Research Start Foundation Project of Jiangsu University (No. 13JDG105), Postgraduate Research & Practice Innovation Program of Jiangsu Province (KYCX19_1601).

Conflicts of Interest: The authors declare no conflict of interest.

References

1. Wenye, W.; Yongguang, H.; Shuo, Y.; Kangqian, M.; Xiaoyong, Z.; Pingping, L. Optimal design of wind machine impeller for frost protection based on CFD and its field test on airflow disturbance. *Int. J. Agric. Biol. Eng.* **2015**, *8*, 43–49.
2. Zhao, R.; Li, H.; Zhang, D.; Huang, J.; Shi, W. Numerical investigation of pump performance and internal characteristics in ALIP with different winding schemes. *Int. J. Appl. Electromagn. Mech.* **2018**, *57*, 39–51. [CrossRef]
3. Fangwei, X.; Rui, X.; Gang, S.; Cuntang, W. Flow characteristics of accelerating pump in hydraulic-type wind power generation system under different wind speeds. *Int. J. Adv. Manuf. Technol.* **2017**, *92*, 189–196. [CrossRef]
4. Nelson, V.; Clark, R.; Foster, R. *Wind Water Pumping*; West Texas A&M University: Canyon, TX, USA, 2004; p. 108.
5. Vick, B.D.; Clark, R.N. Performance of wind-electric and solar-PV water pumping systems for watering livestock. *J. Sol. Energy Eng.* **1996**, *118*, 212–216. [CrossRef]
6. Muljadi, E.; Bergey, M.; Flowers, L.; Green, J. Electric design of wind-electric water pumping systems. *J. Sol. Energy Eng.* **1996**, *118*, 246–252. [CrossRef]
7. Yanxiang, Z.; Zhizhang, L.; Tianqiang, H.; Maofeng, G. Research on wind pumping system and parameter matching. *Renew. Energy* **2006**, *23*, 67–69.
8. Lin, Z.-X.; Huo, T.-Q. Experimental study on water system of wind power pump. *J. Inn. Mong. Univ. Technol. Nat. Sci. Ed.* **2009**, *28*, 139–141.
9. Li, S.-H. *Non-Design Conditions of Vane Pump and Its Optimal Design*; Mechanical Industry Press: Beijing, China, 2006.
10. Neumann, B. *The Interaction between Geometry and Performance of a Centrifugal Pump*; Mechanical Engineering Publications: Beijing, China, 1991.
11. Gao, J.-Y.; Guo, Z.-M. Optimization research on geometric parameters of centrifugal pump impeller and spiral case design. *Pump Technol.* **2007**, *4*, 6–9.
12. Tan, M.-G.; Liu, H.-L.; Yuan, S.-Q. Calculation of hydraulic loss of centrifugal pump. *J. Jiangsu Univ. (Nat. Sci. Ed.)* **2007**, *5*, 11.
13. Korakianitis, T.; Hamakhan, I.A.; Rezaienia, M.A.; Wheeler, A.P.; Avital, E.J.; Williams, J.J. Design of high-efficiency turbomachinery blades for energy conversion devices with the three dimensional prescribed surface curvature distribution blade design (CIRCLE) method. *Appl. Energy* **2012**, *89*, 215–227. [CrossRef]
14. Ouchbel, T.; Zouggar, S.; Elhafyani, M.L.; Seddik, M.; Oukili, M.; Aziz, A.; Kadda, F.Z. Power maximization of an asynchronous wind turbine with a variable speed feeding a centrifugal pump. *Energy Convers. Manag.* **2014**, *78*, 976–984. [CrossRef]
15. Ji, L.; Li, W.; Shi, W. Influence of different blade numbers on unsteady pressure pulsations of internal flow field in mixed-flow pump. *J. Drain. Irrig. Mach. Eng.* **2017**, *35*, 666–673.
16. Yang, M.; Wang, D.; Gao, B.; Lu, S. Influences of guide vane-casing volute positions on performance of nuclear reactor coolant pump. *J. Drain. Irrig. Mach. Eng.* **2016**, *34*, 110–114.
17. Goto, A.; Nohmi, M.; Sakurai, T.; Sogawa, Y. Hydrodynamic design system for pumps based on 3-D CAD, CFD and inverse design method. *ASME J. Fluids Eng.* **2002**, *124*, 329–335. [CrossRef]
18. Passrucker, H.; Van den Braembussche, R.A. Inverse design of centrifugal impellers by simultaneous modification of blade shape and meridional contour. In *ASME Turbo Expo 2000: Power for Land, Sea, and Air*; American Society of Mechanical Engineers: New York, NY, USA, 2000.
19. Zhou, L.; Shi, W.; Lu, W.; Hu, B.; Wu, S. Numerical investigations and performance experiments of a deep-well centrifugal pump with different diffusers. *ASME J. Fluids Eng.* **2012**, *134*, 071102. [CrossRef]

20. Mu, X.-F. *Research and Application of Multidisciplinary Design Optimization Agent Model Technology*; Nanjing Aerospace University: Nanjing, China, 2004.
21. Yuan, S.-Q.; Cao, W.-L. Design of non-overload centrifugal pump by orthogonal test. *Pump Technol.* **1991**, *3*, 1–16.
22. Shi, W.; Zhou, L.; Lu, W.; Zhang, L.; Wang, C. Orthogonal test and optimization design of high lift deep well centrifugal pump. *J. Jiangsu Univ. (Nat. Sci. Ed.)* **2011**, *32*, 400–404.
23. Chunlin, W.; Haibo, P.; Jian, D.; Binjuan, Z.; Fei, J. Optimization design of swirling pump based on response surface method. *J. Agric. Mach.* **2013**, *44*, 59–65.
24. Cheng, J.-L.; Zhen, M.; Lou, J.-Q. Comparison of common experimental optimization design methods. *Lab. Res. Explor.* **2012**, *7*, 7–11.
25. He, X.H.; Cai, S.C.; Deng, Z.D.; Yang, S. Experimental and numerical study of flow characteristics of flat-walled diffuser/nozzles for valveless piezoelectric micropumps. *Proc. Inst. Mech. Eng. Part C J. Mech. Eng. Sci.* **2017**, *231*, 2313–2326. [CrossRef]
26. Kang, C.; Mao, N.; Pan, C.; Zhu, Y.; Li, B. Effects of short blades on performance and inner flow characteristics of a low-specific-speed centrifugal pump. *Proc. Inst. Mech. Eng. Part A J. Power Energy* **2017**, *231*, 290–302. [CrossRef]
27. Kai, W.; Zixu, Z.; Linglin, J.; Houlin, L.; Yu, L. Research on unsteady performance of a two-stage self-priming centrifugal pump. *J. Vibroeng.* **2017**, *19*, 1732–1744. [CrossRef]
28. He, Z.; Pan, Y. Factor test, comparative study of RSM and Taguchi method. *Mech. Des.* **1999**, *16*, 1–4.
29. Wang, K. *Hydraulic Design and Optimization of Centrifugal Pump under Multiple Working Conditions and Its Application*; Jiangsu University: Jiangsu, China, 2011.
30. Weidong, S.; Pingping, Z.; Desheng, Z.; Ling, Z. Unsteady flow pressure fluctuation of high-specific-speed mixed-flow pump. *J. Agric. Eng.* **2011**, *27*, 147–152.